New Journal of Physics
The open access journal at the forefront of physics

Deutsche Physikalische Gesellschaft DPG
IOP Institute of Physics

Published in partnership with: Deutsche Physikalische Gesellschaft and the Institute of Physics

OPEN ACCESS

RECEIVED
27 June 2022

REVISED
17 August 2022

ACCEPTED FOR PUBLICATION
30 August 2022

PUBLISHED
21 October 2022

PAPER

Locating sources of complex quantum networks

Wang Hongjue* and **Zhang Fangfeng**

School of Information, Beijing Wuzi University, Beijing, 101149, People's Republic of China
* Author to whom any correspondence should be addressed.

E-mail: wanghongjue@bwu.edu.cn

Keywords: continuous quantum walk, quantum networks, source location, complex networks

Abstract

The source location of quantum network is an important basic research in the direction of quantum networks, which has important scientific and application values in the frontier fields include quantum state tomography, quantum computing, quantum communication, etc. In this paper, we conduct innovative research on quantum network source location algorithm and theory. A matrix vectorization technique is used to establish a linear system evolution model for quantum network system, and then a high-precision and high-efficiency source location algorithm based on compressed sensing is proposed for large-scale complex quantum networks. All the results of numerical simulation on various model and real networks show the effectiveness and feasibility of the proposed algorithm.

1. Introduction

In recent years, with the development of quantum communication and quantum computing, the research on quantum networks based on quantum walk has attracted much attention and relevant research achievements have been emerging [1]. Quantum network source location is the use of partial observations of quantum network to locate quantum message source nodes. From the perspective of system control, quantum network source location can also be viewed as using the partially observable information of a quantum network system to infer its initial state. The development of efficient source location algorithms for large-scale quantum networks is of great importance.

Quantum state tomography is the use of output information of quantum system to infer the input quantum states, which is a fundamental problem in the field of quantum information [2] and is closely related to quantum network source location. Most of the existing quantum state tomography techniques are applicable to quantum systems with small size and rarely use quantum walk for modeling and analysis. Quantum network source location can be used as a theoretical model for quantum state tomography, which will provide new ideas for developing new high-precision and high-efficiency quantum state tomography techniques and provide theoretical support for traditional techniques to deal with large-scale quantum systems. The essence of quantum computing can be seen as the transfer of a quantum message reversible quantum logic gates [3], and quantum network source location has important potential applications in quantum computing. The preparation of high-quality superposed states is an important step before performing quantum computing [4], and the quality of the superposed states directly affects the efficiency and accuracy of the measurement of computational results. By establishing the quantum network system evolution model of the superposed state, and performing quantum network source location operation, the quality check of the superposed state can be realized. In addition, quantum network source location has potential applications for detecting cascade failures in quantum networks and locating the source of quantum message.

Farhi [5] first proposed the concept of the continuous quantum walk and investigated its efficiency on decision tree problems. In recent years, continuous quantum walk has been widely used in areas such as simulating the operation mechanism of quantum systems [6] and quantum message transfer process [6, 7], developing general quantum computing models [3], and defining the centrality of network nodes [8, 9]. In addition, the relationship between quantum network topology and quantum message propagation

mechanism has been explored, including the effect of network structure on the ability of nodes to transmit quantum message [10], on the efficiency of quantum message propagation [11, 12], on the probability of quantum message distribution on nodes [9, 13], and the relationship between quantum network mediostructure and quantum message transmission [14], etc. In summary, most of the existing research on quantum networks has been carried out mainly from the perspective of direct problems, and few research achievements focus on the inverse problem, that is, the source location of quantum networks.

In the past decade, the research on the source location of classical message propagation processes on complex networks has made great progress [15, 16]. Due to the complexity and variability of practical requirements, researchers have gradually launched more in-depth research. The focus of attention has continuously shifted from tree-structured network source location to general networks with complex topology structures [17–19], from single-source location to multi-source cases [20–23], and the source location of specific propagation models to universal source location algorithms applicable to different propagation models [24]. Existing classical message source location algorithms for complex networks have been prosperous, but they are all limited to classical message propagation models, and a few research focus on quantum message with entangled states, superposed states, immeasurable value and other properties. Although the existing complex network source location algorithms cannot be directly applied to the source location of quantum networks, some algorithms can provide good inspiration for source location of quantum networks. First, the research contents of complex network source location can be extended to quantum networks, including source location accuracy of different network structures, algorithmic efficiency problems, multi-source location problems, etc. Secondly, from the perspective of linear system evolution, the reference [25] proposed a complex network source location algorithm based on compressed sensing. In fact, quantum messages in quantum networks is also generally sparse at the initial time, and if a linear evolution model of quantum network systems is established, the compressed sensing theory is also well suited for developing quantum network source location algorithms.

There is still a lack of analytical research on the intrinsic connection between classical complex network source location and quantum network source location, and there is a lack of efficient source location algorithms and theories applicable to large-scale quantum networks. In this paper, we first establish a linear evolution model of quantum network system with observable quantities by using matrix vectorization technique based on the propagation mechanism of quantum message. And then, after simplifying the linear evolution model, we propose a high-precision and high-efficiency source location algorithm applicable to large-scale quantum networks according to compressed sensing theory.

The rest of this paper is arranged as follows. First, we introduce basic concepts related to quantum network source location. Second, we establish the linear evolution model of quantum network system and propose the multi-source location algorithm. Third, for large-scale quantum network source location, we simplify the proposed algorithm of single source and multi-source cases respectively. Finally, we conclude this paper.

2. Locating sources of quantum network

Consider an arbitrary un-weighted and undirected connected network $G = (V, E)$, where the vertex set V has $N = |V|$ nodes, and the edge set E has $M = |E|$ edges. Self-connection and multiple links are un-allowed. The connection of the network G can be represented as an adjacency matrix A, and its element $a_{i,j}$ is 1 when a link between nodes v_i and v_j exists and 0 otherwise. If $a_{i,j} = 1$, nodes v_i and v_j are neighbor to each other. In matrix A, the sum of elements in line i is the degree of node v_i, which is the number of neighbors of node v_i, diagonal matrix D is the degree matrix of G and the diagonal element $d_{i,i}$ of D is the degree of node v_i. G is a quantum network when a quantum walker located at the nodes of V, and the time evolution of the quantum walker is governed by the Schrödinger equation [9] $\mathrm{i}\hbar\frac{\mathrm{d}}{\mathrm{d}t}|\psi(t)\rangle = H|\psi(t)\rangle$, where H is the Hamiltonian of the isolated quantum system, encoding the structure of G, we use $H = D^{-\frac{1}{2}}LD^{-\frac{1}{2}}$ follow reference [13], and $L = D - A$ is the Laplacian matrix of G, $|\rangle$ is the Dirac notation, representing a state vector, $\hbar$ is reduced Planck constant and we set $\hbar = 1$. The state space of the quantum walker is a N-dimensional Hilbert space spanned by the basis states $|i\rangle = [0, \ldots 0, 1, 0, \ldots, 0]^{\mathrm{T}} (i = 1, 2, \ldots, N)$ which corresponding to node v_i is the unit vector with N elements and the vector that is zero except for a 1 in the ith element. So the state of the quantum walker at time t is $|\psi(t)\rangle = \sum_{i=1}^{N} \alpha_i(t)|i\rangle$, and $\alpha_i(t)$ is complex number, which is the probability amplitude of $|i\rangle$ at time t, and $\alpha_i(t)$ satisfies the normalization condition $\sum_{i=1}^{N} |\alpha_i(t)|^2 = \langle\psi|\psi\rangle = 1$, $|\alpha_i(t)|^2$ is the probability that the quantum walker is found at node v_i after time t, $\langle|$ represents the conjugate transpose of state vector $|\rangle$, $\langle\alpha|\beta\rangle$ represents the inner product of two vectors. The general solution of the Schrödinger equation is

$$|\psi(t)\rangle = U(t)|\psi(0)\rangle, \tag{1}$$

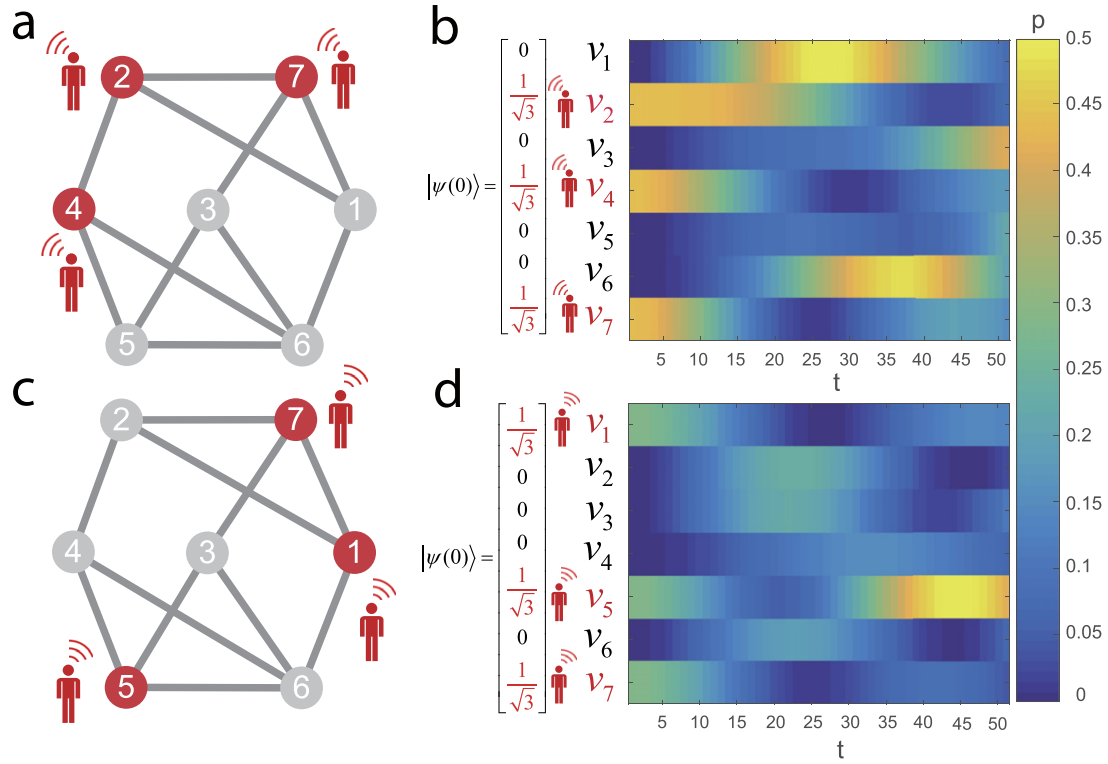

Figure 1. An example of quantum network system and its evolution. (a)–(d) Are examples of the evolution of a quantum system consisting of a quantum walker and a simple network with six nodes. Numbers in the center of nodes are the serial numbers of nodes, and the red nodes are sources of the quantum network, that is, the quantum walker in the superposition state of these nodes at the initial time. In (a), sources of the quantum network are nodes v_2, v_4 and v_7. (b) Is the evolution process of the system in (a), the initial state vector of the system is $|\psi(0)\rangle = \left[0, \frac{1}{\sqrt{3}}, 0, \frac{1}{\sqrt{3}}, 0, 0, \frac{1}{\sqrt{3}}\right]^{\mathrm{T}}$, that is, the probability of the walker at each source at the initial time is equal, i.e. $\frac{1}{3}$. In this paper, unless otherwise specified, it is assumed that the probabilities of the walker on different sources at the initial time are equal. The colors in the heat map correspond to the probabilities of the walker at each node during the evolution process, and these probabilities are measurable quantities, and the abscissa is the time step of the system evolution. It can be seen that during the evolution process, the probability of quantum walker appearing at each node changes over time. (c) and (d) Show the evolution when the walker is in the superposition state of nodes v_1, v_5 and v_7 at the initial time, that is, the source nodes of the network are v_1, v_5 and v_7.

where $U(t) = \mathrm{e}^{-\mathrm{i}Ht}$ and $\mathrm{e}^X = \sum_{k=0}^{\infty} \frac{1}{k!} X^k$. Time t is a continuous real number, in order to be able to simulate continuous quantum walks with computer, we use arbitrarily small numbers to discretize the time t, and we denote $U(1)$ as U which is a unitary matrix with $N \times N$ dimension. In fact, all $U(t)$ for any t are unitary matrices. Figure 1 is an example of quantum network system and its evolution.

In addition, another way to describe the state of a quantum system is using a $N \times N$ density matrix, which is defined as $\rho = |\psi\rangle\langle\psi|$. The main diagonal element $\rho_{i,i}$ of the density matrix is the probability of quantum walker being at node v_i, so the trace of the density matrix is 1. Because the density matrix [26] can describe all the measurable information of the system, the representation of the density matrix is equivalent to that of the wave function for a closed quantum system. Therefore, we can also use density matrix to describe the state of quantum network system. Then the evolution equation for the system becomes

$$\rho(t) = U^t \rho(0) (U^{-1})^t. \tag{2}$$

3. Quantum network source location model based on compressed sensing

Locating sources of quantum network is using probabilities of quantum walker being at a fraction of nodes for some time t to infer the position of non-zero elements in the initial state $|\psi(0)\rangle$ of the quantum walker. This is different from the quantum state tomography which is to infer the initial state $|\psi(0)\rangle$. Because the probability amplitude in $|\psi(t)\rangle$ is unmeasurable, we cannot locate sources by using formula (1) to get $|\psi(0)\rangle = (U(t))^{-1}|\psi(t)\rangle$. Fortunately, the elements in the main diagonal of density matrix $\rho(t)$ is the measurable quantity which is the probability that the quantum walker at each node. Then we will establish a linear evolution model of the quantum network system by vectorizing density matrix, and propose the source location model by compressed sensing theory.

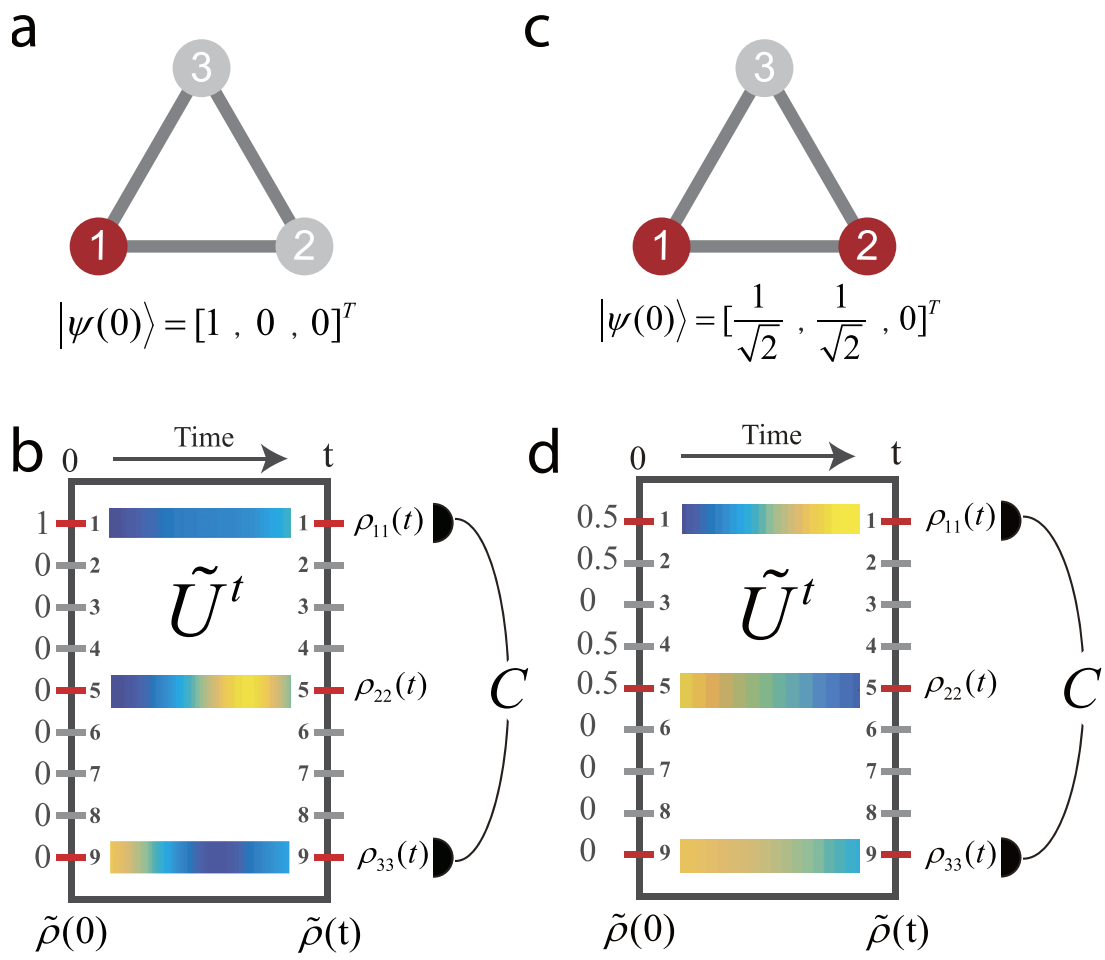

Figure 2. An example of vectorizing density matrix and quantum network source location framework. (a) and (c) Are examples of a quantum system consisting of a quantum walker and a simple network with three nodes. Numbers in the center of nodes are the serial numbers of nodes, and the red nodes are sources of the quantum network, that is, the quantum walker in the superposition state of these nodes at the initial time. In (a), the source node is v_1, so the initial state of the system is $|\psi(0)\rangle = [1, 0, 0]^{\mathrm{T}}$, and the corresponding density matrix is $\rho(0) = \begin{bmatrix} 1 & 0 & 0 \\ 0 & 0 & 0 \\ 0 & 0 & 0 \end{bmatrix}$. (b) Is the observer information after the evolution of the system in (a). The leftmost side is the vectorized density matrix $\tilde{\boldsymbol{\rho}}(0)$ with nine elements, and the elements marked in red correspond to the probability that the walker appearing at each node, that is, the elements on the main diagonal of $\rho(0)$. After the system has evolved by $\tilde{U}^t$, we observe the probability that the walker locating at nodes v_1 and v_3 at time t, and the observer matrix is $C = \begin{bmatrix} 1 & 0 & 0 & 0 & 0 & 0 & 0 & 0 & 0 \\ 0 & 0 & 0 & 0 & 0 & 0 & 0 & 0 & 1 \end{bmatrix}$. The observer nodes are v_1 and v_3, so the dimension of matrix C is 2×3^2, and the first row of C is used to obtain the probability that the quantum walker being at the observer node v_1, and the second row is used to obtain the probability of the quantum walker being at observer node v_3, the position number of the 1 in the first row is $(i^{o_1} \cdot N + i^{o_1} - N) = 1 \times 3 + 1 - 3 = 1$, and the position number of 1 in the second row is $(i^{o_3} \cdot N + i^{o_3} - N) = 3 \times 3 + 3 - 3 = 9$. In (c), the quantum walker is in the superposition state of nodes v_1 and v_2 at the initial time, that is, the source nodes are v_1 and v_2, the initial state of the system is $|\psi(0)\rangle = \left[\frac{1}{\sqrt{2}}, \frac{1}{\sqrt{2}}, 0\right]^{\mathrm{T}}$, and the corresponding density matrix is $\rho(0) = \begin{bmatrix} 0.5 & 0.5 & 0 \\ 0.5 & 0.5 & 0 \\ 0 & 0 & 0 \end{bmatrix}$. If we observe nodes v_1 and v_2 at the initial time, we will detect the quantum walker on nodes v_1 and v_2 with probability 0.5. (d) Is the observer information after the evolution of the system in (c).

We first define $\tilde{U} = U^{\dagger} \otimes U$, where $U^{\dagger}$ is the conjugate matrix of U, $\otimes$ denote direct product, so the dimension of $\tilde{U}$ is $N^2 \times N^2$. Then we vectorize $\rho(t)$ as

$$\tilde{\boldsymbol{\rho}}(t) = \begin{bmatrix} \rho_{11}(t) \\ \rho_{21}(t) \\ \vdots \\ \rho_{N1}(t) \\ \rho_{12}(t) \\ \rho_{22}(t) \\ \vdots \\ \rho_{NN}(t) \end{bmatrix}, \tag{3}$$

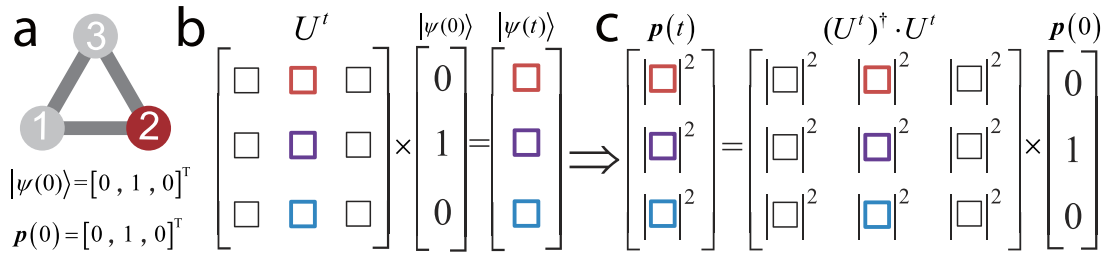

Figure 3. The diagram of simplified single source location model. (a) Is an example of a quantum system consisting of a quantum walker and a simple network with three nodes. Numbers in the center of nodes are the serial numbers of nodes, and the red node v_2 is source of the quantum network, so the initial state of the system is $|\psi(0)\rangle = [0,1,0]^{\mathrm{T}}$, and the corresponding probability is $\boldsymbol{p}(0) = [0,1,0]^{\mathrm{T}}$. (b) After the evolution of U^t, the obtained state $|\psi(t)\rangle$ is actually the elements in the second column of U^t, which is corresponding to node v_2, so the corresponding probabilities are moduli of the elements in the second column of U^t. Therefore, for the case of single source location, we can convert the evolution model of the system to the form in (c), that is, the elements in evolution matrix are moduli of the elements in unitary matrix U^t, and the probability amplitude in the state vector is replaced by probability.

Table 1. Detailed information of model networks. ⟨degree⟩ is the average degree of a network. ⟨distance⟩ is the average distance of network and ⟨distance⟩ $= \frac{1}{N(N-1)}\sum_{i,j} d_{v_i,v_j}$, where d_{v_i,v_j} is the distance between nodes v_i and v_j.

Name	Parameters for generating network	Parameters for generating network	N	⟨degree⟩	⟨distance⟩
BA	Power exponent	0.5	300	4	2
		1	300	4	3
		1.5	300	4	3.3
		2	500, 300	4	3.8
		0.005	300	2	14
		0.008	500	4	5
ER	Adding link probability	0.01	300	3	5
		0.015	300	4	4
		0.02	300	6	3
		0.025	300	8	3
		0.1	300	4	7
WS	Removing link probability	0.2	300	4	5.5
		0.3	300	4	5
		0.4	500, 300	4	5
		0.5	300	4	4.5

where the $(i \cdot N + i - N)$-th element in $\tilde{\boldsymbol{\rho}}(t)$ is the probability of quantum walker locate at node v_i at time t. So we get the linear evolution model for the quantum network system as

$$\tilde{\boldsymbol{\rho}}(t+1) = \tilde{U}\tilde{\boldsymbol{\rho}}(t), \tag{4}$$

where $\widetilde{(U^t)} = (U^t)^\dagger \otimes (U^t) = (U^\dagger)^t \otimes (U^t) = (U^\dagger \otimes U)^t = (\tilde{U})^t$, so $\tilde{\boldsymbol{\rho}}(t) = (\tilde{U})^t\tilde{\boldsymbol{\rho}}(0)$.

Suppose we can only observe the probabilities of quantum walker locate at n observer nodes $O = \{o_1, o_2, \ldots, o_n\}$ at some discrete time steps, and the probabilities at time t is denoted by $\boldsymbol{p}_O(t) = [p_1(t), p_2(t), \ldots, p_n(t)]^{\mathrm{T}}$, then the source location model is

$$\begin{bmatrix} \boldsymbol{p}_O(t_0+t) \\ \boldsymbol{p}_O(t_0+t+1) \\ \vdots \\ \boldsymbol{p}_O(t_0+t+k-1) \end{bmatrix} = \begin{bmatrix} C\tilde{U}^{t_0+t} \\ C\tilde{U}^{t_0+t+1} \\ \vdots \\ C\tilde{U}^{t_0+t+k-1} \end{bmatrix} \tilde{\boldsymbol{\rho}}(t_0), \tag{5}$$

where t_0 is the initial time which is known in advance, unless otherwise specified, this paper takes $t_0 = 0$, t is the time to start the observation, and continuously observe k time steps. C is a $n \times N^2$ output matrix, in the ith line of C, only the $(i^{o_i} \cdot N + i^{o_i} - N) -$ th element is 1 and other elements are 0, and $o_i = v_{i^{o_i}}$. For a quantum network, the maximum dimension of the output matrix C that we can take is $N \times N^2$, that is, the probability of quantum walker locating at all nodes are observed. An example of obtaining matrix C is shown in figure 2(b). Since most of the elements in $\tilde{\boldsymbol{\rho}}(t_0)$ are 0, that is, $\tilde{\boldsymbol{\rho}}(t_0)$ is a sparse vector, the model can be analyzed by compressive sensing theory, and can be solved by lasso or dual interior point method [27]. This paper use dual interior point method. Figure 2 is an example of vectorizing density matrix and quantum network source location framework.

Table 2. Detailed information of real networks.

Name	N	M	⟨degree⟩	⟨distance⟩	Description of networks
Political blogs [31]	1222	16 714	27.36	2.74	Hyper links between web logs on US politics
Airline [32]	332	2126	12.81	2.74	US air transportation network
Neural [33]	297	2148	14.46	2.46	Neural network of *Caenorhabditis elegans*
Jazz [31]	198	2742	5.12	2.24	A network of jazz bands
Football [34]	115	613	10.66	2.51	The network of USA football games in the fall of 2000
Santa Fe [35]	118	200	3.37	5.12	Scientific collaboration network of the Santa Fe Institute

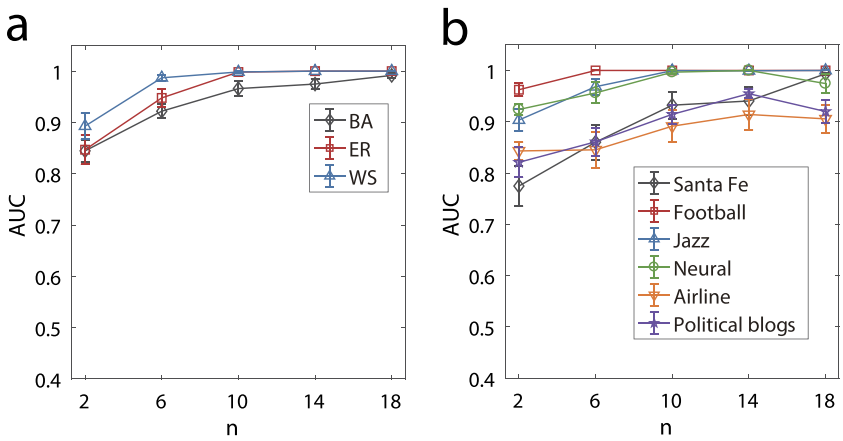

Figure 4. Accuracy of locating single source for different model and real networks. Abscissa is the number of observer nodes and ordinate is AUC value. Error bars represent the standard error. Curves of different colors corresponding to different complex networks. (a) Model networks. (b) Real networks.

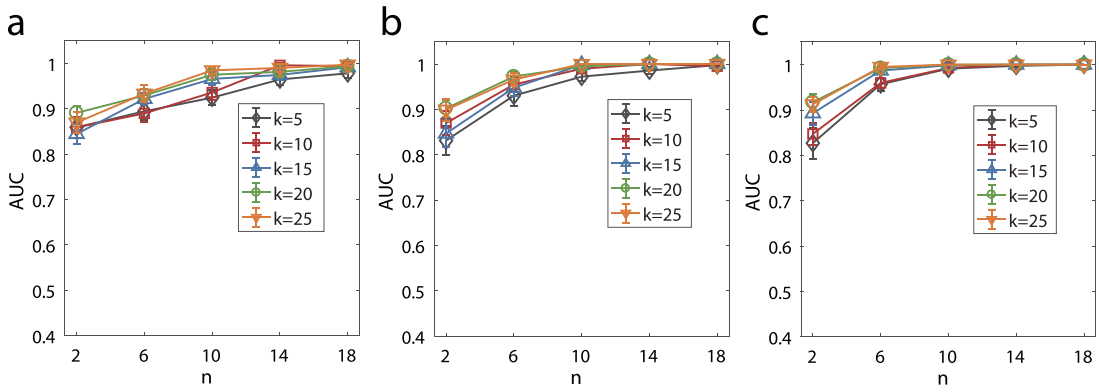

Figure 5. Accuracy of locating single source for different observer time steps on model networks. Abscissa is the number of observer nodes and ordinate is AUC value. Error bars represent the standard error. Curves of different colors corresponding to different time steps. (a) BA. (b) ER. (c) WS.

4. Simplified sources location model for large scale quantum networks

After vectorize density matrix, we successfully convert equation (2) to a linear evolution model (4), and proposed a compressed sensing theory based sources location model (5). While, after the vectorization operation, the unitary evolution matrix change from $N \times N$ dimensional U to $N^2 \times N^2$ dimensional $\tilde{U}$, and this result in high complexity of sources location model for large scale complex networks. Furthermore, a mass of complex numbers will influence solution accuracy and then reduce source location accuracy. In view of these difficulties, we consider to reasonably simplify source location model (5) in this section.

4.1. Simplified single source location model

Single source means that the initial state of the quantum walker is locate at only one node of network G. Suppose the initial source node is v_i, then the initial state is $|i\rangle$ that only the ith element is 1 and other

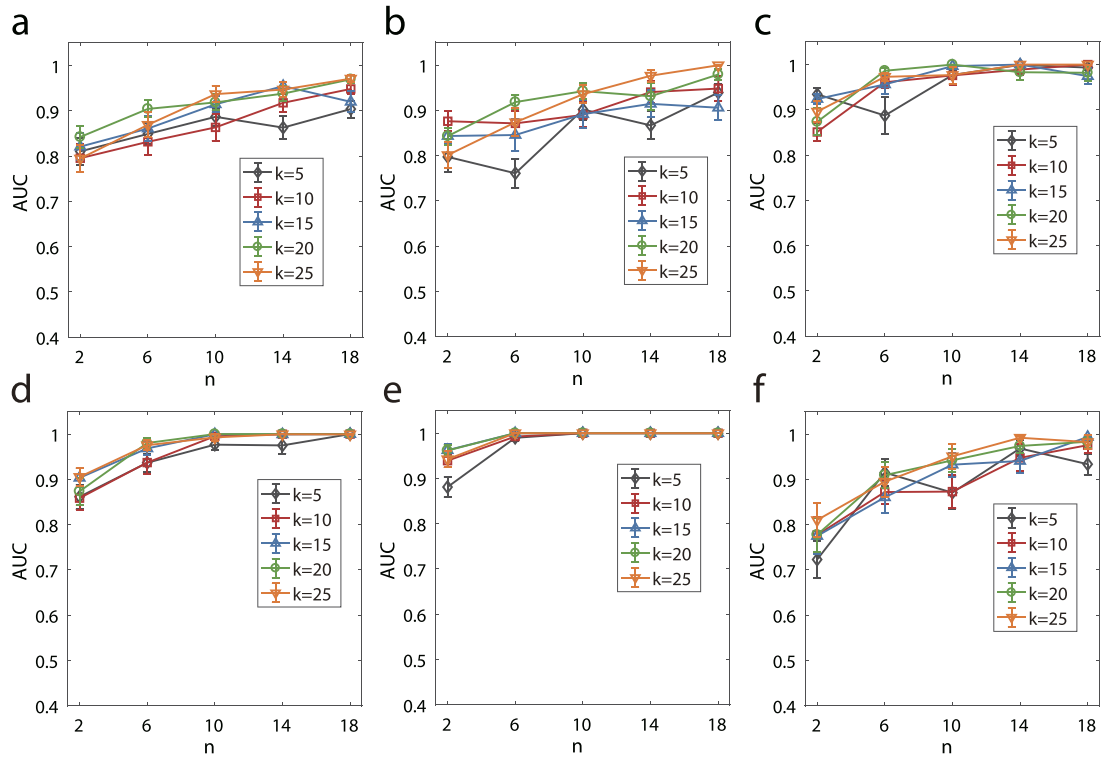

Figure 6. Accuracy of locating single source for different observer time steps on real networks. Abscissa is the number of observers nodes and ordinate is AUC value. Error bars represent the standard error. Curves of different colors corresponding to different time steps. (a) Political blogs. (b) Airline. (c) Neural. (d) Jazz. (e) Football. (f) Santa Fe.

elements are 0, after the evolution of unitary matrix U, we get the next state is

$$|\psi\rangle = U|i\rangle = U\begin{bmatrix}\vdots\\0\\1\\0\\\vdots\end{bmatrix} = \begin{bmatrix}U_{1,i}\\\vdots\\U_{i,i}\\\vdots\\U_{N,i}\end{bmatrix} \tag{6}$$

so the measurable probabilities of quantum walker locating at nodes is $\boldsymbol{p}_V = \left[|U_{1,i}|^2, |U_{2,i}|^2, \ldots, |U_{n,i}|^2\right]$. Where $\left|U_{j,i}\right|^2$ is the modulus of a complex element $U_{j,i}$. Therefore, for the single source case, we get the following evolution equation of quantum network system as

$$\boldsymbol{p}_V(t) = (U^t)^\dagger \cdot U^t \boldsymbol{p}_V(0), \tag{7}$$

where the $N \times N$ matrix $\hat{U}(t) = (U^t)^\dagger \cdot U^t$ represents the elements at the corresponding positions of the two matrices are multiplied. So the source location model is

$$\begin{bmatrix}\boldsymbol{p}_O(t_0+t)\\\boldsymbol{p}_O(t_0+t+1)\\\vdots\\\boldsymbol{p}_O(t_0+t+k-1)\end{bmatrix} = \begin{bmatrix}C\hat{U}(t_0+t)\\C\hat{U}(t_0+t+1)\\\vdots\\C\hat{U}(t_0+t+k-1)\end{bmatrix} p_V(t_0). \tag{8}$$

Figure 3 is the diagram of simplified single source location model.

In order to quantify the validity and efficiency of the proposed source locating algorithm based on limited observer nodes, we study the success rate of locating sources on both model and real networks. Model networks are BA scale-free network (BA) [28], ER random network (ER) [29]and WS small world network (WS) [30]. See table 1 for more detailed parameters and properties of model network. Real static networks including political blogs, airline. Neural, jazz, football and Santa Fe and detailed information of these real networks are shown in table 2. During simulations in this paper, observer nodes and sources are selected randomly except where noted. Here a standard metric, area under the receiver operating

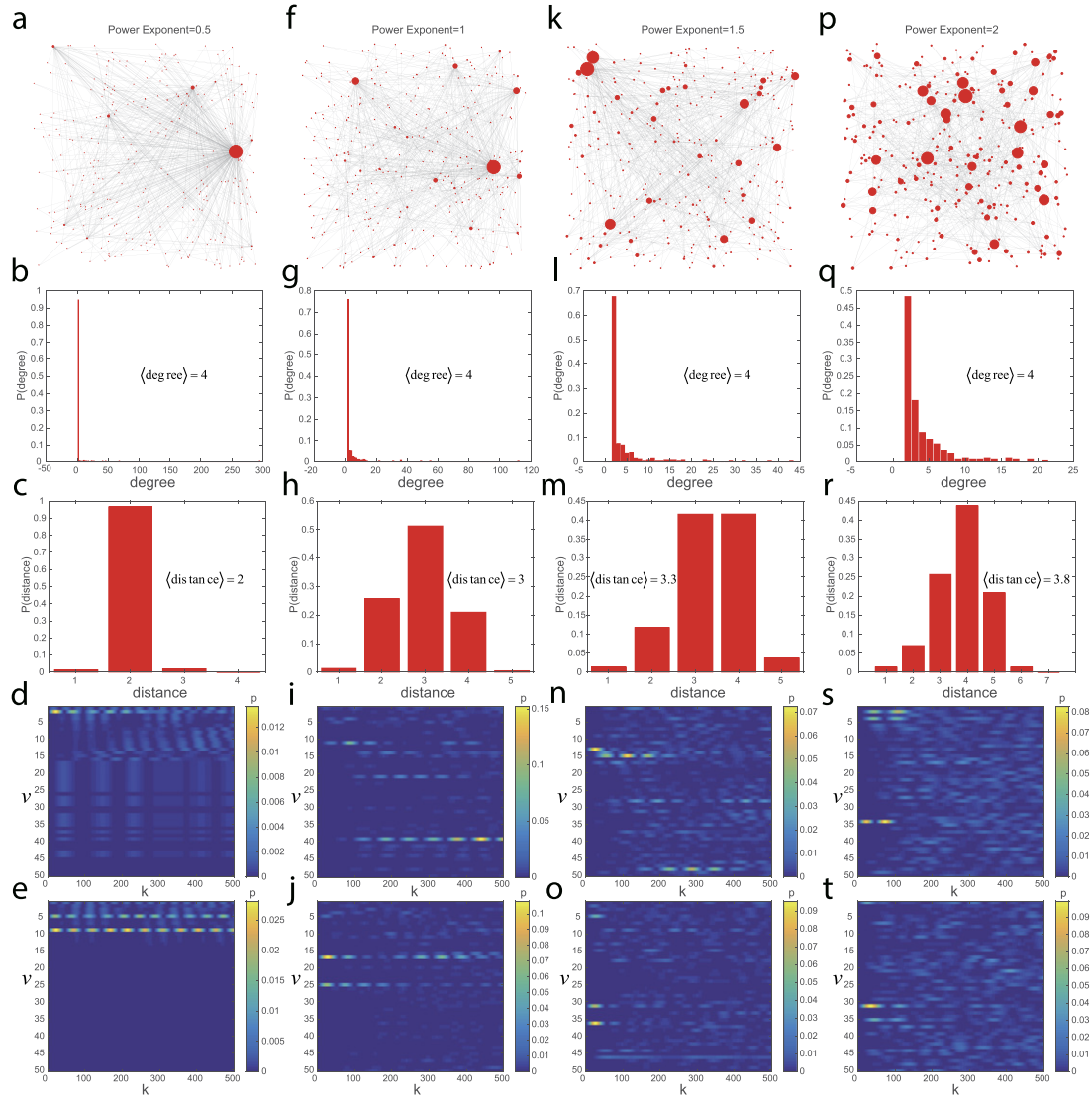

Figure 7. Network topology, network properties and quantum walk probability distribution of BA model networks with size $N = 300$. (a) Is the topology of the BA network with power exponent of 0.5, (b) and (c) are the degree distribution and distance distribution of the network in (a) respectively, (d) and (e) are the heat map of probability distribution of quantum walker locating at network nodes after 500 time-step quantum walks, only nodes with the top 50 labels are displayed, (d) is the probability distribution of the quantum walk after randomly selecting one source, (e) is the probability distribution of randomly selecting two sources. (f)–(j) Are the case of BA network with power exponent of 1, (k)–(o) are the case of BA network with power exponent of 1.5, (p)–(t) are the case of BA network with power exponent of 2.

characteristic curve (AUC) [24] is used to quantify the accuracy of our algorithm. We first rank the nodes based on their reconstructed probability values in $\boldsymbol{p}_V(t_0)$ in ascending order and result in a new candidate list. AUC value is calculated by two indexes, true positive rate (TPR) and false positive rate (FPR). $\mathrm{TPR}(l) = \frac{\mathrm{TP}(l)}{s}$, where $\mathrm{TP}(l)$ is the number of true sources in the top l nodes of candidate list, s is the number of sources. $\mathrm{FPR}(l) = \frac{\mathrm{FP}(l)}{N-s}$, where $\mathrm{FP}(l)$ is the number of false positives in the top l nodes of candidate list. The abscissa of receiver operating characteristic curve is FPR and ordinate is TPR, AUC is the area under this curve. The higher value of AUC, the better locating performance of algorithm. All results AUC are mean value of 200 repetitive simulations.

Figures 4–6 are the simulation results of simplified single source location on model networks with size $N = 500$ and average degree $\langle \mathrm{degree} \rangle = 4$ and empirical networks. See table 1 for more detailed parameters and properties of model network with size $N = 500$. Figure 4 shows the accuracies of source locating on model and real networks with time step $k = 15$. As we can see, the performance of our method increase with the number of observers nodes increasing. Clearly, for all different model networks, only approximately $6(6/500 = 1.2\%)$ observer nodes can receive relatively high accuracy AUC > 0.9. For all different real networks in figure 4(b), we can obtain AUC > 0.8 by only six observer nodes. Figures 5 and 6 are the accuracy of locating source for different observer time steps on model and real networks respectively. Clearly, from figure 5, in model networks, precisely locate the source of BA network is the most difficult, for

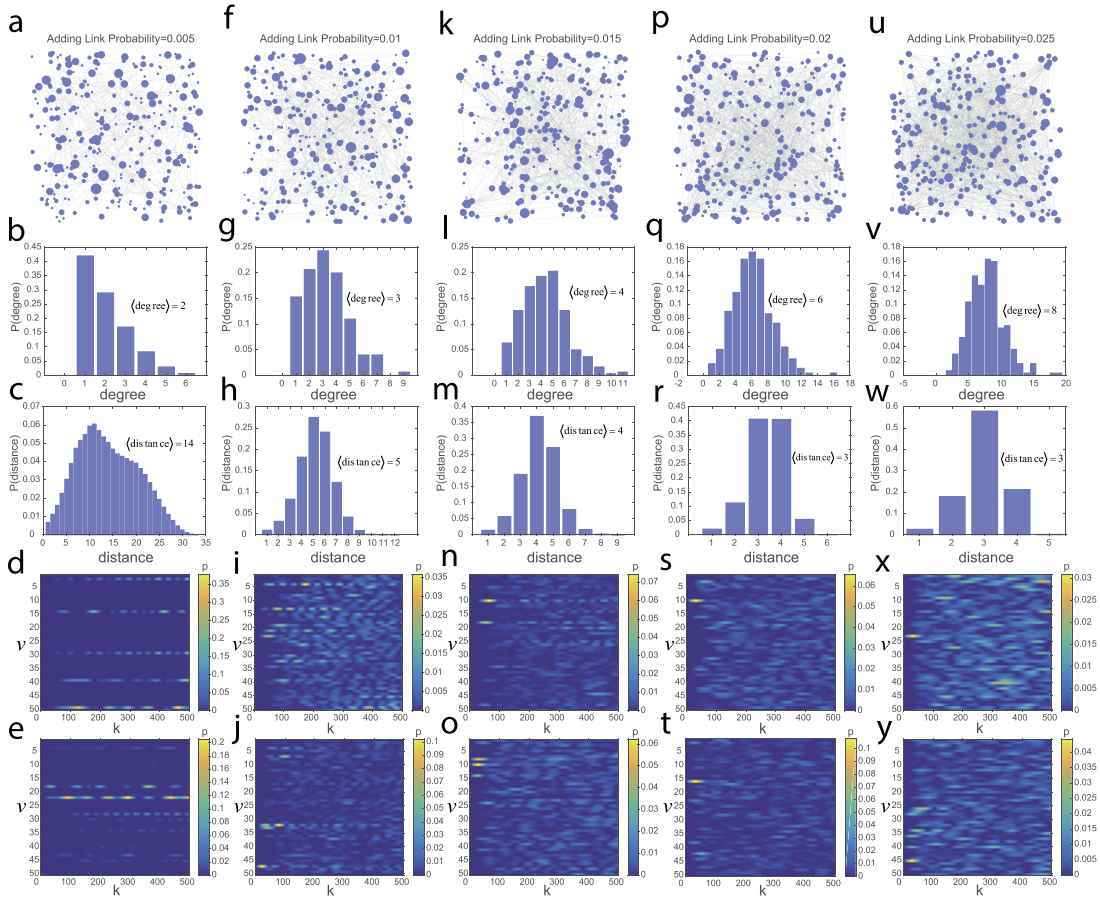

Figure 8. Network topology, network properties and quantum walk probability distribution of ER model networks with size $N = 300$. (a) Is the topology of the ER network with adding link probability of 0.005, (b) and (c) are the degree distribution and distance distribution of the network in (a) respectively, (d) and (e) are the heat map of probability distribution of quantum walker locating at network nodes after 500 time-step quantum walks, only nodes with the top 50 labels are displayed, (d) is the probability distribution of the quantum walk after randomly selecting one source, (e) is the probability distribution of randomly selecting two sources. (f)–(j) Are the case of ER network with adding link probability of 0.01, (k)–(o) are the case of ER network with adding link probability of 0.015, (p)–(t) are the case of ER network with adding link probability of 0.02, (u)–(y) are the case of ER network with adding link probability of 0.025.

all different time steps on model networks, only approximately $2(2/500 = 0.4\%)$ observer nodes can receive relatively high accuracy AUC > 0.8 and receive AUC > 0.9 by using $10(10/500 = 2\%)$ observer nodes. From figure 6, for all real networks, precisely locate the source of airline is more difficult than others, only approximately ten observer nodes can receive relatively high accuracy AUC > 0.8 for all different time steps, especially on football network can obtain AUC > 0.9 for only six observer nodes. In addition, for most model and real networks, different time steps have little effect on source location precision.

In addition, in order to study the influence of different parameters of model networks and observer node selection strategies on source location accuracy, we selected BA scale-free networks with size $N = 300$ and different power exponents as 0.5, 1, 1.5 and 2, ER random networks with size $N = 300$ and different adding link probabilities as 0.005, 0.01, 0.015 0.02 and 0.025, and WS small world networks with size $N = 300$ and different removing link probabilities as 0.1, 0.2, 0.3, 0.4 and 0.5. See table 1 and figures 7–9 for more detailed parameters and properties of model network with size $N = 300$. The source location accuracy by different observer nodes selection strategies is compared and analyzed. The observer nodes selection strategies include: random selection (randomly select n nodes as observer nodes), maximum degree (selecting the n nodes with the largest degree as observer nodes), maximum closeness centrality (selecting the n nodes with the largest closeness centrality as observer nodes), maximum betweenness (selecting the n nodes with the largest betweenness as observer nodes), maximum PageRank centrality (selecting the n nodes with the largest PageRank centrality as observer nodes) and maximum eigenvector centrality (selecting the n nodes with the largest eigenvector centrality as observer nodes). Figure 10 shows the influence of different observer nodes selection strategies and network parameters on the single source location accuracy. In the simulation process, we select the number of observer nodes as $n = 10$, the observer time step as $k = 10$, and randomly selected one source. For single source location, it can be seen from figure 10(a) that, according to the mean value of AUC value, when the power exponent of BA network

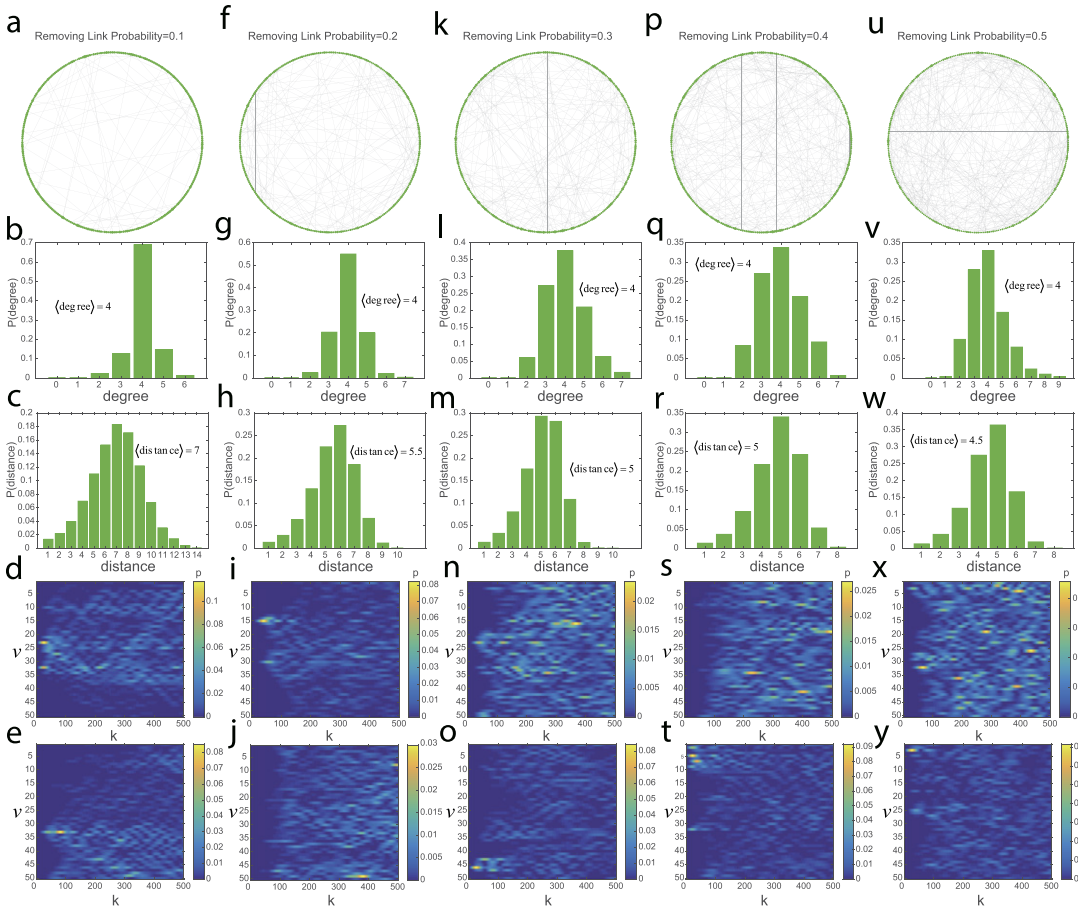

Figure 9. Network topology, network properties and quantum walk probability distribution of WS model networks with size $N = 300$. (a) Is the topology of the WS network with removing link probability of 0.1, (b) and (c) are the degree distribution and distance distribution of the network in (a) respectively, (d) and (e) are the heat map of probability distribution of quantum walker locating at network nodes after 500 time-step quantum walks, only nodes with the top 50 labels are displayed, (d) is the probability distribution of the quantum walk after randomly selecting one source, (e) is the probability distribution of randomly selecting two sources. (f)–(j) are the case of WS network with removing link probability of 0.2, (k)–(o) are the case of WS network with removing link probability of 0.3, (p)–(t) are the case of WS network with removing link probability of 0.4, (u)–(y) are the case of WS network with removing link probability of 0.5.

is 0.5, maximum closeness centrality strategy perform best and random selection has the worst performance. For power exponents 1, 1.5 and 2, in addition to random selection strategy, all other observer nodes selection strategies have satisfactory source location results. In figure 10(b), when the adding link probability of ER network is 0.005, the source location result of maximum degree strategy is the best, and the maximum eigenvector centrality strategy is the worst. For other adding link probabilities, the source location accuracy of all strategies is satisfactory. In figure 10(c), when the removing link probability of WS network is 0.1, the source location accuracy of maximum PageRank strategy is the highest, and the maximum eigenvector centrality is the worst. For other removing link probabilities, the source location accuracy of all strategies is satisfactory. As can be seen from figure 10(d), with the increase of parameters of different model networks, the source location accuracy increases. In general, the proposed simplified single source location algorithm can perform well on different model and real networks.

4.2. Simplified multi-source location model

Multi-source mean that the initial state of the quantum walker is concurrently locate at multiple nodes of network G with a superposed state. In this case, we first analyze and simplify model (4), and then get the corresponding simplified source location model. In order to simplify model (4), we firstly apply the similarity transformation to matrix $\tilde{U}$, that is exchanging the rows and columns of the matrix $\tilde{U}$ at the same time and finally obtain a block matrix with the following form

$$\bar{U} = \begin{bmatrix} U^{\dagger} \cdot U & \Delta_1 \\ \Delta_2 & \Delta_3 \end{bmatrix}, \tag{9}$$

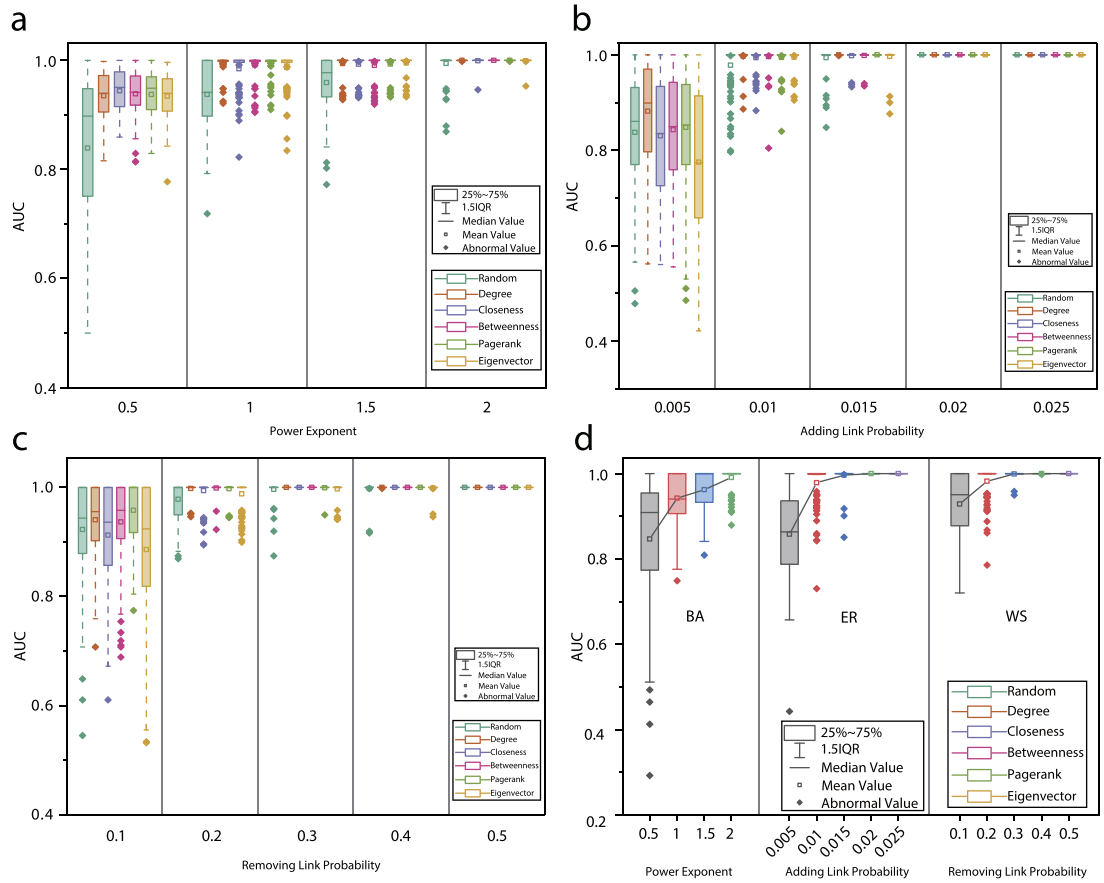

Figure 10. Influence of different observer nodes selection strategies and generation parameters of model networks on single source location accuracy. (a) Is the influence of different observer nodes selection strategies on the single source location accuracy for BA networks. (b) Is the influence of different observer nodes selection strategies on the single source location accuracy for ER networks. (c) Is the influence of different observer nodes selection strategies on the single source location accuracy for WS networks. (d) Is the influence of different network generation parameters on the single source location accuracy.

where Δ_1, Δ_2 and Δ_3 represent the other blocks. The corresponding $\tilde{\boldsymbol{\rho}}$ of $\tilde{U}$ becomes the following form

$$\bar{\boldsymbol{\rho}}(t) = \begin{bmatrix} \rho_{11}(t) \\ \rho_{22}(t) \\ \vdots \\ \rho_{NN}(t) \\ \vdots \end{bmatrix} \tag{10}$$

So we get the evolution equation

$$\bar{U}\bar{\boldsymbol{\rho}}(t) = \begin{bmatrix} U^{\dagger} \cdot U & \Delta_1 \\ \Delta_2 & \Delta_3 \end{bmatrix} \begin{bmatrix} \rho_{11}(t) \\ \rho_{22}(t) \\ \vdots \\ \rho_{NN}(t) \\ \vdots \end{bmatrix} = \begin{bmatrix} \rho_{11}(t+1) \\ \rho_{22}(t+1) \\ \vdots \\ \rho_{NN}(t+1) \\ \vdots \end{bmatrix}. \tag{11}$$

Then we omit Δ_2 and Δ_3, and replace Δ_1 with a $N \times N$ identity matrix I, then we get the simplified approximate evolution of model (4) as

$$\bar{U}\bar{\boldsymbol{\rho}}(t) = \left[U^{\dagger} \cdot U, I\right] \begin{bmatrix} \rho_{11}(t) \\ \rho_{22}(t) \\ \vdots \\ \rho_{NN}(t) \\ \Omega(t) \end{bmatrix} = \begin{bmatrix} \rho_{11}(t+1) \\ \rho_{22}(t+1) \\ \vdots \\ \rho_{NN}(t+1) \end{bmatrix}, \tag{12}$$

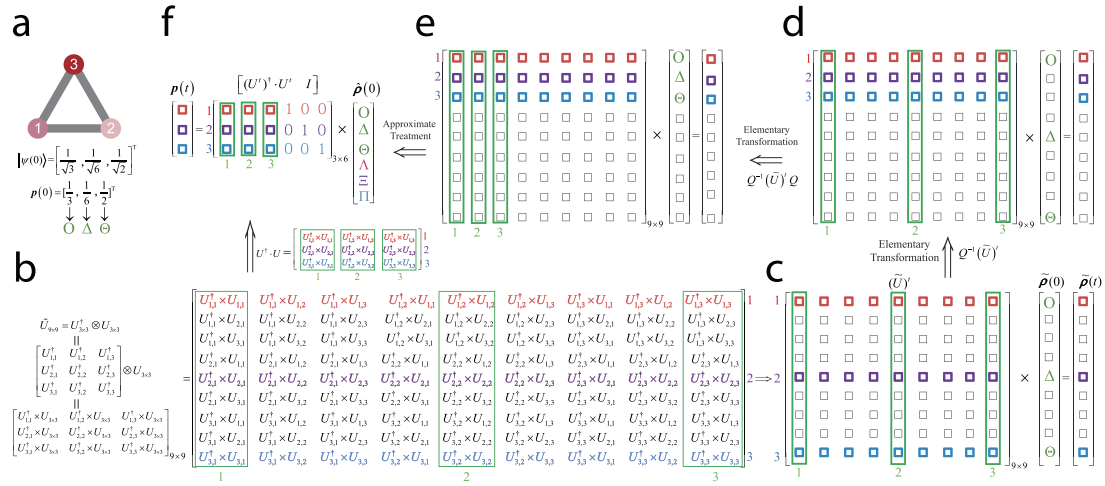

Figure 11. The diagram of simplified multi-source location model. (a) An example of a quantum system consisting of a quantum walker and a simple network with three nodes. Numbers in the center of nodes are the serial numbers of nodes, and the red nodes v_1, v_2 and v_3 are sources of the quantum network, that is, the quantum walker in the superposition state of these nodes at the initial time, so the initial state of the system is $|\psi(0)\rangle = \left[\frac{1}{\sqrt{3}}, \frac{1}{\sqrt{6}}, \frac{1}{\sqrt{2}}\right]^{\mathrm{T}}$, and the corresponding probability is $\boldsymbol{p}(0) = \left[\frac{1}{3}, \frac{1}{6}, \frac{1}{2}\right]^{\mathrm{T}}$, the shade of nodes color is proportional to the probability. We use three green symbols O, Δ and Θ represent the probability of nodes v_1, v_2 and v_3 in $\boldsymbol{p}(0)$ respectively. (b) Is diagram of calculating $\tilde{U}_{9\times9}$ of network in (a). The three rows numbered 1 (red), 2 (purple) and 3 (blue) in $\tilde{U}_{9\times9}$ and the three columns numbered 1, 2, 3 and marked with green generate $U^{\dagger}\cdot U$ by their intersecting elements. (c) Is the system evolution equation of (a). The three rows numbered 1 (red), 2 (purple) and 3 (blue) in $\tilde{U}^t$ are respectively operated with $\tilde{\boldsymbol{\rho}}(0)$ to get the elements in $\tilde{\boldsymbol{\rho}}(t)$ which are marked as O (red), Δ (purple) and Θ (blue). In the product operation of matrix$\tilde{U}^t$ and vector $\tilde{\boldsymbol{\rho}}(0)$, the three columns numbered 1, 2, 3 in $\tilde{U}^t$ and marked with green will be multiplied by the three green symbols O, Δ and Θ in $\tilde{\boldsymbol{\rho}}(0)$ respectively. (d) Is obtained by elementary row transformation Q^{-1} of $\tilde{U}^t$ in (b), that is, the rows in $\tilde{U}^t$ are exchanged, and the rows marked 1 (red), 2 (purple), and 3 (blue) are arranged at the front, then the corresponding probability in $\tilde{\boldsymbol{\rho}}(t)$ is also at the top. (e) Is to perform elementary column transformation Q on the evolution matrix in (c), that is, exchange the columns of $Q^{-1}\tilde{U}^t$, so that the columns 1, 2, and 3 marked in green are ranked at the forefront, and the corresponding probability in $\tilde{\boldsymbol{\rho}}(0)$ is also ranked at the top. After (b) to (d), the similar transformation of matrix $\tilde{U}^t$ is completed, and the probabilities in $\tilde{\boldsymbol{\rho}}(0)$ and $\tilde{\boldsymbol{\rho}}(t)$ are ranked at the top. (f) Is an approximate simplification of (d). Only the part of the probability value is retained in $\tilde{\boldsymbol{\rho}}(t)$, and then replaced with $\boldsymbol{p}(t)$, so only the first three rows of elements are retained in the evolution matrix $Q^{-1}(\tilde{U})^t Q$ after similarity transformation, and the elements of the non-probability part in $\tilde{\boldsymbol{\rho}}(0)$ are simplified to three elements, marked with three symbols Λ (red), Ξ (purple) and Π (blue), and denote the part of the evolution matrix corresponding to these three symbols as an identity matrix I. So the final simplified evolution equation is

$$\left[(U^t)^{\dagger}\cdot U^t, I\right]\begin{bmatrix}\rho_{11}(0)\\ \rho_{22}(0)\\ \vdots\\ \rho_{NN}(0)\\ \Omega(0)\end{bmatrix} = \begin{bmatrix}\rho_{11}(t)\\ \rho_{22}(t)\\ \vdots\\ \rho_{NN}(t)\end{bmatrix} = \boldsymbol{p}(t) \text{ or } \left[U^{\dagger}\cdot U, I\right]\begin{bmatrix}\rho_{11}(t)\\ \rho_{22}(t)\\ \vdots\\ \rho_{NN}(t)\\ \Omega(t)\end{bmatrix} = \begin{bmatrix}\rho_{11}(t+1)\\ \rho_{22}(t+1)\\ \vdots\\ \rho_{NN}(t+1)\end{bmatrix} = \boldsymbol{p}(t+1), \text{ where } \Omega = \begin{bmatrix}\Lambda\\ \Xi\\ \Pi\end{bmatrix}.$$

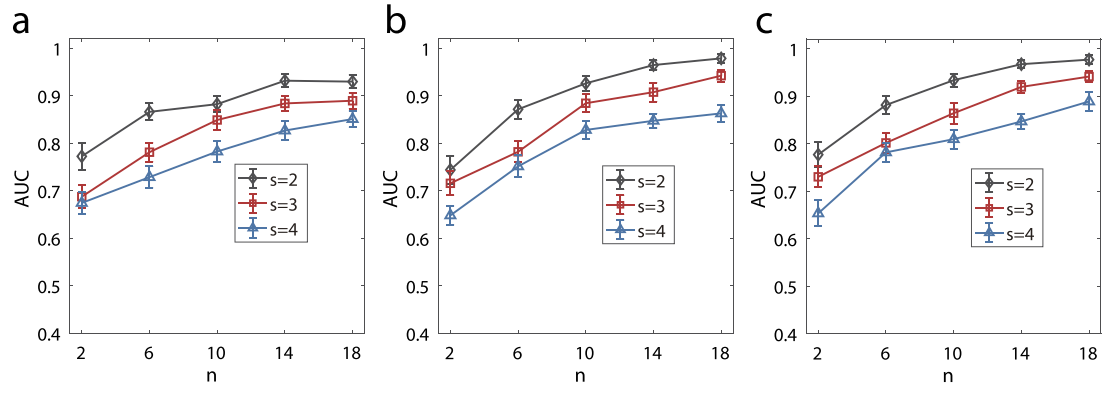

Figure 12. Accuracy of locating multi-source for different number of sources on model networks. Abscissa is the number of observer nodes and ordinate is AUC value. Error bars represent the standard error. Curves of different colors corresponding to different number of sources. (a) BA. (b) ER. (c) WS.

where the dimension of $\bar{U} = \left[U^{\dagger}\cdot U, I\right]$ is $N \times 2N$, $\Omega(t)$ is an unknown vector with N elements, so the dimension of $\bar{\boldsymbol{\rho}}(t)$ is $2N \times 1$. In fact, we simplify the model by combining the unmeasurable quantities into $\Omega(t)$ and remaining all N measurable quantities. Model (12) is the logical approximation of model (4) without changing its evolution principle, and which also dramatically reduce computational and space

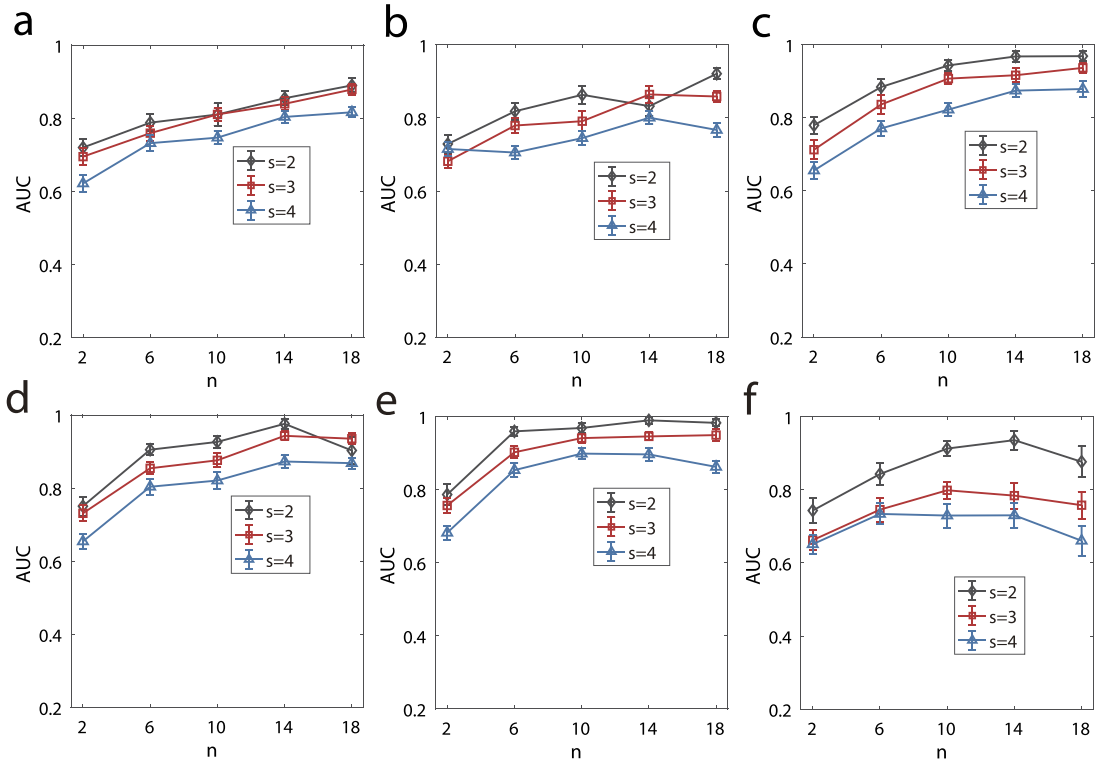

Figure 13. Accuracy of locating multi-source for different number of sources on real networks. Abscissa is the number of observer nodes and ordinate is AUC value. Error bars represent the standard error. Curves of different colors corresponding to different number of sources. (a) Political blogs. (b) Airline. (c) Neural. (d) Jazz. (e) Football. (f) Santa Fe.

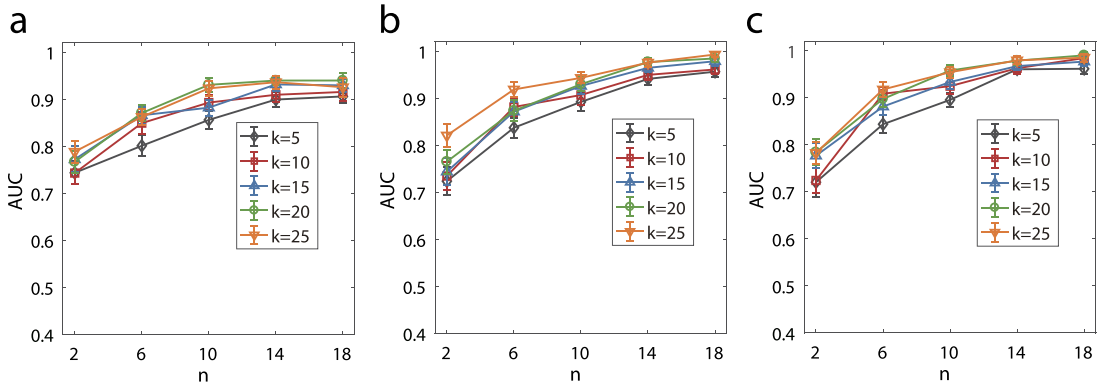

Figure 14. Accuracy of locating multi-source for different observer time steps on model networks. Abscissa is the number of observer nodes and ordinate is AUC value. Error bars represent the standard error. Curves of different colors corresponding to different time steps. (a) BA. (b) ER. (c) WS.

complexity. We denote $\left[(U^t)^\dagger \cdot U^t, I\right]$ as $\bar{U}(t)$, so the simplified source location model is

$$\begin{bmatrix} \boldsymbol{p}_O(t_0+t) \\ \boldsymbol{p}_O(t_0+t+1) \\ \vdots \\ \boldsymbol{p}_O(t_0+t+k-1) \end{bmatrix} = \begin{bmatrix} C\bar{U}(t_0+t) \\ C\bar{U}(t_0+t+1) \\ \vdots \\ C\bar{U}(t_0+t+k+1) \end{bmatrix} \bar{\boldsymbol{\rho}}(t_0). \tag{13}$$

Figure 11 is the diagram of simplified multi-source location model. Figures 12–14 are the simulation results of the proposed multi-source location algorithm on model networks with size $N = 500$ and average degree $\langle \text{degree} \rangle = 4$ and empirical networks. See table 1 for more detailed parameters and properties of model network with size $N = 500$. Figure 12 shows the accuracies of locating multi-source for different number of sources on model networks with $k = 15$. As we can see, the performance of our method increase with the number of observers nodes increasing. And with the increase of number of sources, locating source

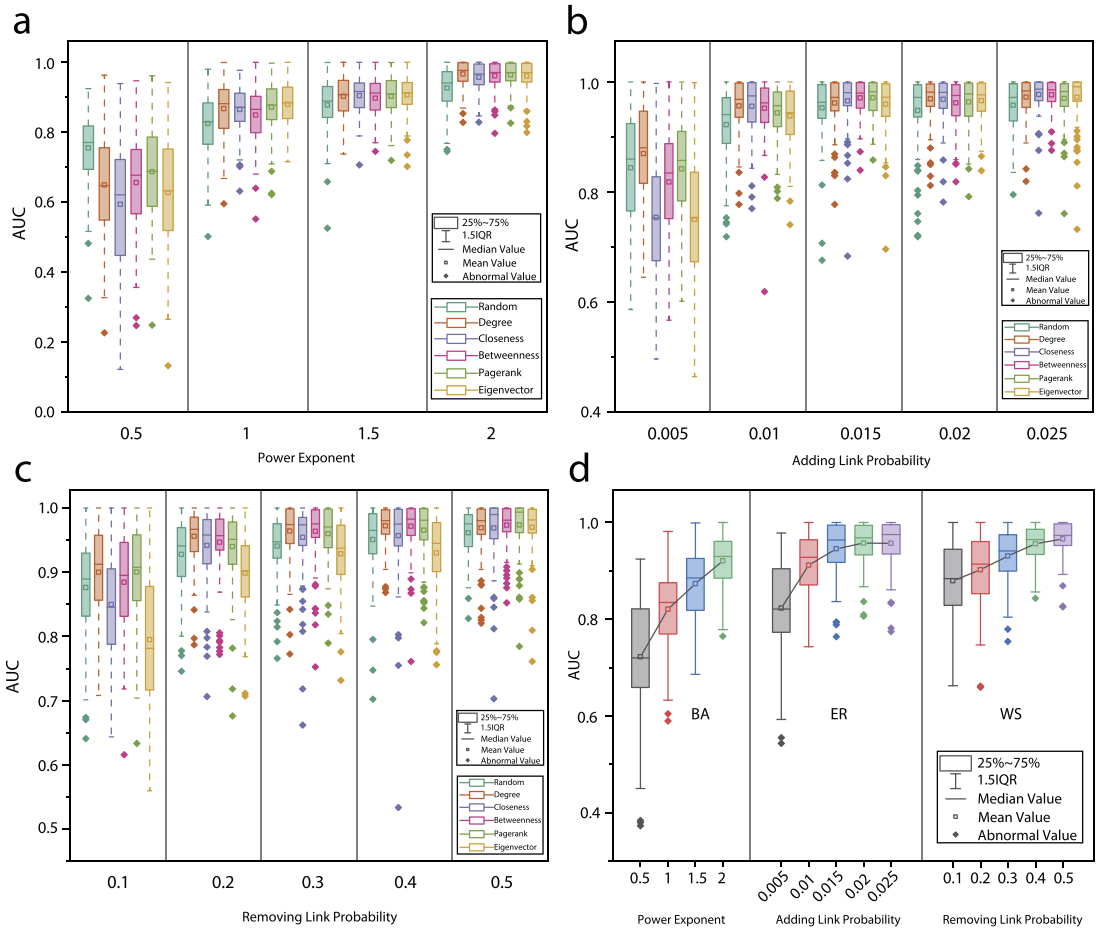

Figure 15. Influence of different observer nodes selection strategies and generation parameters of model networks on multi-source location accuracy. (a) Is the influence of different observer nodes selection strategies on multi-source location accuracy for BA networks. (b) Is the influence of different observer nodes selection strategies on the multi-source location accuracy for ER networks. (c) Is the influence of different observer nodes selection strategies on the multi-source location accuracy for WS networks. (d) Is the influence of different network generation parameters on multi-source location accuracy.

accurately becomes more difficult. Figure 13 shows the accuracies of multi-source location for different number of sources on real networks with $k = 15$. Figure 14 are the accuracy of locating multi-source with $s = 2$ for different observer time steps on model networks. Clearly, from figure 14, for all different time steps on model networks, only approximately $2(2/500 = 0.4\%)$ observer nodes can receive relatively high accuracy AUC > 0.7. Figure 15 shows the influence of different observer nodes selection strategies and network parameters on the multi-source location accuracy. In the simulation process, we select the number of observer nodes as $n = 10$, the observer time step as $k = 10$, and randomly selected two source. For multi-source location, it can be seen from figure 15(a) that, according to the mean value of AUC value, when the power exponent of BA network is 0.5, random selection strategy perform best and maximum closeness centrality has the worst performance. For power exponents 1, 1.5 and 2, in addition to random selection strategy, all other observer nodes selection strategies have satisfactory source location results. In figure 15(b), when the adding link probability of ER network is 0.005, the source location result of maximum degree strategy is the best, and the maximum eigenvector centrality strategy is the worst. For other adding link probabilities, the source location accuracy of all strategies is satisfactory. In figure 15(c), when the removing link probability of WS network are 0.1, 0.2, 0.3 and 0.4, the source location accuracy of maximum degree strategy is the highest, and the maximum eigenvector centrality is the worst. For removing link probability 0.5, the source location accuracy of all strategies is satisfactory. As can be seen from figure 15(d), with the increase of parameters of different model networks, the source location accuracy increases. In general, the performance of the proposed multi-source location algorithm is satisfactory.

5. Discussions

In this paper, we propose a high-precision and high-efficiency multi-source location algorithm based on compressive sensing for large-scale complex quantum networks. The proposed algorithm can accurately locate all sources by using information of limited observer nodes for model networks with different topologies and real networks. The proposed algorithm also performs satisfactorily according to simulating from the perspectives of different number of observer nodes, different observer time steps, different number of sources and different observer nodes selection strategies. However, the proposed algorithm still have some room for improvement. First, the proposed algorithm locate the source when initial time of sources is known, but the initial time is unknown in most practical cases. Second, the algorithm in this paper can only be applied to closed quantum systems, and the observer information is not affected by noise, but most real quantum systems are more sensitive to external environments, and the observer information is generally unpurified. Third, in this paper, all observer nodes selection strategies are based on network topology, and the number and location of the optimal observer nodes based on integrated factors including characteristics of source location algorithm are still need to be studied further.

Acknowledgments

This work is supported by the Youth Fund of Beijing Wuzi University (Grant No. 2021XJQN05). The authors would like to express sincere appreciation to Wang Wenxu, Xu Hongya, Lai Yingcheng and Sun Kaijia for their detailed and helpful comments to improve the quality of the paper.

Conflict of interest

The authors declare that they have no known competing financial interests or personal relationships that could have appeared to influence the work reported in this paper.

Data availability statement

The data generated and/or analysed during the current study are not publicly available for legal/ethical reasons but are available from the corresponding author on reasonable request.

Credit authorship contribution statement

These authors contributed equally to this work.

ORCID iDs

Wang Hongjue https://orcid.org/0000-0001-6226-347X

References

[1] Biamonte J, Faccin M and De Domenico M 2019 Complex networks from classical to quantum *Commun. Phys.* **2** 53
[2] Oren D, Mutzafi M, Eldar Y C and Segev M 2017 Quantum state tomography with a single measurement setup *Optica* **4** 993–9
[3] Childs A M 2009 Universal computation by quantum walk *Phys. Rev. Lett.* **102** 180501
[4] Wollack E A, Cleland A Y, Gruenke R G, Wang Z, Arrangoiz-Arriola P and Safavi-Naeini A H 2022 Quantum state preparation and tomography of entangled mechanical resonators *Nature* **604** 463–7
[5] Farhi E and Gutmann S 1998 Quantum computation and decision trees *Phys. Rev.* A **58** 915
[6] Mareš J, Novotnỳ J and Jex I 2020 Quantum walk transport on carbon nanotube structures *Phys. Lett.* A **384** 126302
[7] Martín-Vázquez G and Rodríguez-Laguna J 2020 Optimizing the spatial spread of a quantum walk *Phys. Rev.* A **102** 022223
[8] Paparo G D, Müller M, Comellas F and Martin-Delgado M A 2014 Quantum Google algorithm *Eur. Phys. J. Plus* **129** 150
[9] Izaac J A, Zhan X, Bian Z, Wang K, Li J, Wang J B and Xue P 2017 Centrality measure based on continuous-time quantum walks and experimental realization *Phys. Rev.* A **95** 032318
[10] Cardillo A, Galve F, Zueco D and Gómez-Gardenes J 2013 Information sharing in quantum complex networks *Phys. Rev.* A **87** 052312
[11] Osada T, Coutinho B, Omar Y, Sanaka K, Munro W J and Nemoto K 2020 Continuous-time quantum-walk spatial search on the Bollobás scale-free network *Phys. Rev.* A **101** 022310
[12] Mülken O and Blumen A 2011 Continuous-time quantum walks: models for coherent transport on complex networks *Phys. Rep.* **502** 37–87

[13] Faccin M, Johnson T, Biamonte J, Kais S and Migdał P 2013 Degree distribution in quantum walks on complex networks *Phys. Rev.* X **3** 041007
[14] Faccin M, Migdał P, Johnson T H, Bergholm V and Biamonte J D 2014 Community detection in quantum complex networks *Phys. Rev.* X **4** 041012
[15] Huang C, Liu X, Deng M, Zhou Y and Bu D 2018 A survey on algorithms for epidemic source identification on complex networks *Chin. J. Comput.* **41** 1156–79
[16] Wang H-J, Zhang F-F and Sun K-J 2021 An algorithm for locating propagation source in complex networks *Phys. Lett.* A **393** 127184
[17] Shah D and Zaman T 2011 Rumors in a network: who's the culprit? *IEEE Trans. Inf. Theory* **57** 5163–81
[18] Wang H-J and Sun K-J 2020 Locating source of heterogeneous propagation model by universal algorithm *Europhys. Lett.* **131** 48001
[19] Pinto P C, Thiran P and Vetterli M 2012 Locating the source of diffusion in large-scale networks *Phys. Rev. Lett.* **109** 068702
[20] Zhu K and Ying L 2014 Information source detection in the sir model: a sample-path-based approach *IEEE/ACM Trans. Netw.* **24** 408–21
[21] Antulov-Fantulin N, Lančić A, Šmuc T, Štefančić H and Šikić M 2015 Identification of patient zero in static and temporal networks: robustness and limitations *Phys. Rev. Lett.* **114** 248701
[22] Jiang J, Wen S, Yu S, Xiang Y and Zhou W 2015 K-center: an approach on the multi-source identification of information diffusion *IEEE Trans. Inf. Forensics Secur.* **10** 2616–26
[23] Fu L, Shen Z, Wang W-X, Fan Y and Di Z 2016 Multi-source localization on complex networks with limited observers *Europhys. Lett.* **113** 18006
[24] Wang H 2019 An universal algorithm for source location in complex networks *Physica* A **514** 620–30
[25] Hu Z-L, Han X, Lai Y-C and Wang W-X 2017 Optimal localization of diffusion sources in complex networks *R. Soc. Open Sci.* **4** 170091
[26] Titchener J G, Solntsev A S and Sukhorukov A A 2016 Two-photon tomography using on-chip quantum walks *Opt. Lett.* **41** 4079–82
[27] Donoho D L 2006 Compressed sensing *IEEE Trans. Inf. Theory* **52** 1289–306
[28] Albert R and Barabási A-L 2002 Statistical mechanics of complex networks *Rev. Mod. Phys.* **74** 47
[29] Barabási A-L and Albert R 1999 Emergence of scaling in random networks *Science* **286** 509–12
[30] Watts D J and Strogatz S H 1998 Collective dynamics of 'small-world' networks *Nature* **393** 440–2
[31] Li F, Jing H, Huang G, Zhang Y and Shi Y 2014 RETRACTED: a clustering-based link prediction method in social networks *Procedia Comput. Sci.* **29** 432–42
[32] Batagelj V and Mrvar A 2006 Pajek datasets: reuters terror news network http://vlado.fmf.uni-lj.si/pub/networks/data/CRA/terror.htm (accessed March 2008).
[33] Lü L and Zhou T 2011 Link prediction in complex networks: a survey *Physica* A **390** 1150–70
[34] Li J, Wang X and Cui Y 2014 Uncovering the overlapping community structure of complex networks by maximal cliques *Physica* A **415** 398–406
[35] Girvan M and Newman M E J 2002 Community structure in social and biological networks *Proc. Natl Acad. Sci. USA* **99** 7821–6